JOURNAL OF PROPULSION AND POWER
Vol. 25, No. 3, May–June 2009

Ground Test Investigation of Temperature Distribution in Four Parallel High-Altitude Engines

Wenbo Qin* and Huier Cheng†
Shanghai Jiao Tong University, 200240 Shanghai, People's Republic of China
and
Peng Li‡
Institute of Shanghai Aerospace System Engineering, 201108 Shanghai, People's Republic of China

DOI: 10.2514/1.38313

This paper describes a ground test investigation of temperature distribution in the vacuum cabin of an engine group with four parallel nozzles when subjected to the high-altitude conditions encountered in space. A new scheme was devised to simulate and evaluate the influence of radiative heat transfer on the wall temperature distribution of high-altitude engines in the vacuum cabin. Nozzles used in the ground test were geometrically and physically analogous to the actual ones used in space. Electric heating nozzles, instead of the actual ones, were used in the test unit. Characteristics of the wall temperature distribution were obtained by measuring the wall temperatures of the four- and two-parallel-nozzle configurations. It was shown from the testing data that, due to the mutual radiation among high-temperature nozzles with small gaps, the maximum circumferential temperature rise, ΔT_{max}, was less than 30K at the throat with high temperature, whereas ΔT_{max} was less than 250K at the exit with low temperature. Thus, the temperature rise of the whole thrust chamber did not affect the normal working of the set of engines. Comparing the data from numerical simulation, it is indicated that the results from the electric heating test in a vacuum cabin are conservative and reliable.

Nomenclature

D_c	=	diameter of the vacuum cabin
d_c	=	diameter of the nozzle's cylinder section
d_t	=	diameter of the throat
Gr	=	Grashof number
H_c	=	height of the vacuum cabin
L_n	=	length of the test nozzle
l	=	eigendimension of the vacuum cabin
P	=	power
p	=	pressure
Q	=	heating power
q	=	heat flux
S	=	diagonal distance of the nozzle group
$T(t)$	=	temperature
α_b	=	mixture ratio in the region near wall
β	=	obliquity of nozzle
ΔT	=	temperature difference
δ	=	wall thickness of the nozzle
ε	=	area ratio or emissivity
θ	=	circular angle

Subscripts

max	=	maximum
min	=	minimum
g	=	combustion gas
el	=	electricity

Received 29 April 2008; revision received 10 November 2008; accepted for publication 18 November 2008.

*Ph.D., Department of Aeronautical and Astronautical Engineering.
†Professor, Department of Aeronautical and Astronautical Engineering.
‡Ph.D.

I. Introduction

AN ALL-RADIATION cooling mode is usually applied to a high-altitude engine that works in a high-vacuum and low-temperature environment; thus, the wall temperature of this kind of thruster chamber is very high [1,2]. If a propulsive system with four parallel engines (see Fig. 1) is used to adjust the orbit of a spacecraft, the radiative heat transfer among high-temperature nozzles with a small gap between them will result in a rise in temperature of the nozzle walls, which may cause burnout. Niu et al. [3] and Cheng and Niu [4] analyzed the influence of outward radiation of four parallel thrust chambers on wall temperature by numerical simulation. At present, no kind of testing has been conducted regarding this problem. Such testing usually requires a high-altitude test bed; however, this test is too expensive, and the wall temperature distribution cannot be acquired easily by use of the infrared radiometer because of cross-nozzle interference. In this work, a new scheme for a ground simulation test will be presented that involves electrically heating the nozzles (hereafter called test nozzles) in the vacuum cabin at normal temperature. The high-temperature distribution characteristics of the four parallel engines can be obtained by directly measuring the circumferential wall temperature of the test nozzles using thermocouples. Common pyrology equipment can be used to evaluate the thermal reliability of the new propulsive scheme with four parallel engines.

II. Design of the Ground Test

To make the temperature measurements of an engine in the ground test consistent with those of an actual engine in space, the test conditions must meet the following three criteria [5]:

1) The geometrical and physical conditions of the two systems are equal or analogical.

2) The physical conditions of the environments in which the two systems exist are equal.

3) The distribution of heat flux on the nozzles is equal.

Therefore, the design of the ground test should meet these three criteria as much as possible. A schematic of test devices for the ground test is shown in Fig. 2. The main test devices will be explained in the following subsections.

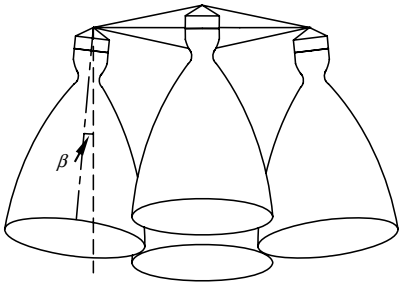

Fig. 1 Radiation system of four parallel engines with small gap.

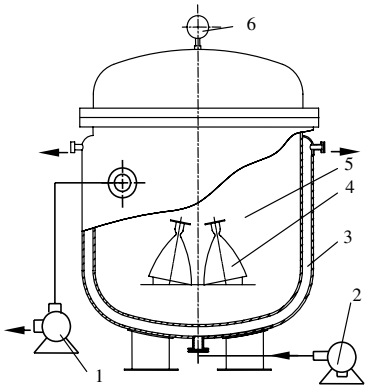

1. Vacuum pump 2. Water pump 3. Jacket
4. Test nozzle 5. Vacuum cabin 6. Vacuum meter

Fig. 2 Schematic of test devices for the ground test of the engine group.

A. Vacuum Cabin

The diameter and height of the vacuum cabin are $D_c = 1600$ mm and $H_c = 2200$ mm, respectively. The main physical parameters in the vacuum cabin are pressure and temperature, which influence radiative heat transfer between nozzles at high temperature, according to the theory of radiative heat transfer [6]. The vacuum in space is equal to $<10^{-4}$ Pa; thus, it is unnecessary to generate such a high vacuum in the vacuum cabin. Only the amount of vacuum necessary to make air natural convection and air molecular conduction negligible is required for high-temperature radiative heat transfer.

It is well known that air heat conduction is at least 1 order of magnitude less than natural convection [5]; thus, air heat conduction could be ignored if natural convection is ignored. Baehr and Stephan [5] indicated that the natural convection can be ignored if the Grashof number is $Gr < 2000$. The cabin pressure can be calculated as $p < 151$ Pa by selecting a conservative representative dimension of the vacuum cabin l, the temperature T, and the temperature difference ΔT as 0.4 m, 400K and 500K, respectively. There are two stages of vacuum pumps in the test system: the mechanical pump and the Roots vacuum pump. The designed vacuum degree is 1 Pa.

It is very difficult to simulate the low space temperature of 4K in the vacuum cabin [7]. For early evaluation, it is more economical, easy, and error tolerant to pump water at a normal temperature of about 27°C instead of liquid nitrogen into the jacket of the vacuum cabin to maintain a normal temperature in the inner wall. Radiation is in direct proportion to the fourth power of the temperature according to Stefan–Boltzmann's law [6]. The ratio is $(300/773)^4 = 2.3\%$ between radiative heat flux from the inner wall of the vacuum cabin at a normal temperature and that from the extension section or exit of a nozzle whose temperature is about 773K [3]. The ratio is less than 0.31% at the throat region of a nozzle with a temperature above 1273K [3]. Thus, errors in the test caused by having the cabin walls at a normal temperature instead of the space environment are negligible from an engineering point of view.

B. Test Nozzles

The four scaled-down nozzles are manufactured from cheaper stainless steel instead of niobium alloy, and the scaling ratio is 0.55. The length of the test nozzle is $L_n = 426$ mm, the diameter of the cylinder section is $d_c = 49.8$ mm, the diameter of the throat is $d_t = 29.8$ mm, the area ratio is $\varepsilon = 88.8$, and the wall thickness is $\delta = 2$ mm. The test nozzle is geometrically analogous to the actual one to maintain consistency in viewing the two systems. A special coating is sprayed on the surface of the test nozzles. The measured emissivity of the coating on the test nozzle and niobium alloy is shown in Table 1. It is indicated that the radiative characteristics of the coating on the test nozzle is the same as that on the niobium alloy below 1000°C. The emissivity of the coating on the test nozzle is a little greater than that on niobium alloy. Additional advantages of the scaled-down nozzles are that the dimensions of the vacuum cabin and the electric heating power can be decreased.

C. Electric Heaters

The wall temperature distribution of the test nozzle is produced by electric heating, not hot gas. It is impossible to get the same axial temperature distribution of the test nozzle as that of an actual one by electric heating because infinite independent electric heaters cannot be installed in the test nozzle. Because the purpose of the test is to perform a preliminary investigation of the thermal reliability of the new propulsive system, three electric heaters that can be independently adjusted in power are placed axially in a test nozzle. According to the contractive and expansive geometrical characteristics and the wall temperature distribution of a nozzle, heater 1 is at the cylinder-convergent section, heater 2 is at the expansion section, and heater 3 is at the extension section (as shown in Fig. 3). A heat insulative plate is placed at the exit of the test nozzle, which can decrease the heat radiation leakage from the exit (see Fig. 3).

The electric heater is composed of a special ceramic core and heating wires. The material of the core is 95% ceramics ($95\%AL_2O_3$), which is able to endure the temperature of 1700°C [8]. The shape of the core is consistent with the inner surface of the nozzle, and the gaps between them are only 0.6–1.0 mm. The heating wires are wound in spiral slots chiseled on the external surface of the cores. The material of the heating wire is iron, chromium, and aluminum alloy (ICAA), which can endure a temperature of 1300°C [9] and have good antioxidation properties at high temperature.

D. Thermocouples for Measuring Temperature

Two sorts of thermocouples are selected according to different temperature levels. The platinum–platinum-rhodium alloy (PRA) thermocouples with the diameter of 0.1 mm are used at the throat at high temperature, and the nickel-chromium alloy–nickel-silicon alloy (NCA–NSA) thermocouples with a diameter of 0.5 mm are used at other positions. All the thermocouples have been calibrated ahead of the test. Thirty-eight thermocouples are placed on four test nozzles to get sufficient temperature data. The concrete positions of thermocouples are explained as follows (see Fig. 4):

1) Nozzle 1 is selected as the one measured in the geometrically symmetrical system (see Fig. 4). Then, 21 thermocouples are placed at special sections of the nozzle to acquire the temperature distribution of the nozzle.

2) The four axial positions for the thermocouples are the end of cylinder section, the throat, the beginning of the extension section

Table 1 Measured emissivity of the coat on test nozzle and niobium alloy

Temperature, °C		400	500	600	700	800	900	1000
Emissivity	On test nozzle	0.89	0.87	0.87	0.85	0.83	0.82	0.81
	On niobium alloy	0.86	0.85	0.84	0.84	0.82	0.81	0.81

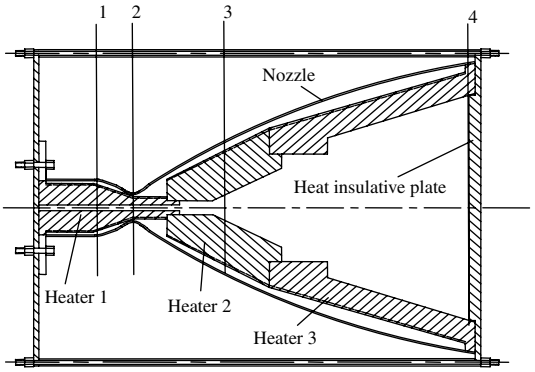

Fig. 3 Electric heating scheme of the test nozzle and axial number of the thermocouples on the outer wall of the nozzle

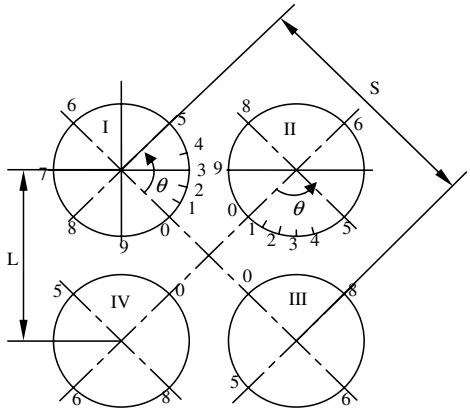

Fig. 4 Circumferential locations of the thermocouples on the outer wall of the nozzles.

($\varepsilon = 9$), and the exit (see Fig. 3). Nine circumferential positions for thermocouples are shown in Fig. 4.

3) Seventeen additional thermocouples are placed at corresponding positions on the other three nozzles.

III. Commissioning of the Test Devices

The purpose of commissioning the test devices is to check the rationality and reliability of the test design. Parameters and test devices have been checked carefully.

1) The test rig is used to place the four test nozzles, whose obliquity and distance among them can be adjusted. The diagonal distance of the nozzle group is $S = 352$ mm and the obliquity is $\beta = 6.73$ deg (see Fig. 1 and 4).

2) The function of the water-cooling system is simply to provide the jacket of the vacuum cabin with sufficient water to maintain a normal temperature of the inner wall. There was no failure in the water-cooling system in the process of the commissioning.

3) The degree of vacuum in the cabin is a key parameter that will influence the test quality. The absolute pressure of the cabin in the test was only kept at the level of 100 Pa, which was 2 orders of magnitude higher than that in the design. The natural convection could be ignored in such a vacuum on the whole. Heating elements that could endure higher temperatures, such as tungsten wire or tantalum, were not used in the vacuum environment.

4) There were many difficulties in the commissioning of an electric heating system. The main problem was that the ICAA wires expanded and slid out of the narrow slots of the ceramic core after they were electrified and heated; then, a short circuit occurred due to the touching of the ICAA wires. Three improvements of the slots were made in the shape, dimension, and direction, and the problem was solved. We attempted to use tungsten wire, which can endure higher temperatures and has a lower linear expansion coefficient. However, the tungsten wire broke immediately after it was electrified, because tungsten wire needs higher vacuum ($p < 0.1$ Pa) [10]. According to the model of radiative heat transfer [11] between two concentric cylinder surfaces, calculations indicated that the wall temperature of the nozzle was equal to 1000°C when the temperature of the ICAA wire was approximately at its melting point of 1300°C. In other words, if the ICAA wire was selected as the heating element, it was estimated that the wall temperature at the throat could reach 1000°C at most.

IV. Test Results and Analyses

First, the two-stage pumps worked in regular order and the pressure in the cabin decreased gradually. Second, electric heaters were operated to preheat the nozzles when the pressure in the cabin reached 100 Pa. The preheating process needed 6–7 h because of the higher heat capacity and lower thermal diffusivity of the ceramic insert in the heaters. Third, operation of the data collecting system began when the throat temperature of a test nozzle reached 300°C. The temperature data of all measured points were collected and recorded every 1 min Finally, the test ended when the throat temperature reached 900–1000°C. The data collecting system ensured the synchronicity in the data measured from the 38 thermocouples. During the test, the absolute pressure of 100 Pa in the vacuum cabin and its inner wall temperature of 300K were maintained. The four nozzles have approximately the same temperature distributions. At the same position on each test nozzle, it was found that the minimum temperature difference was 2K and the maximum was 14K. This proves that the measured data are credible.

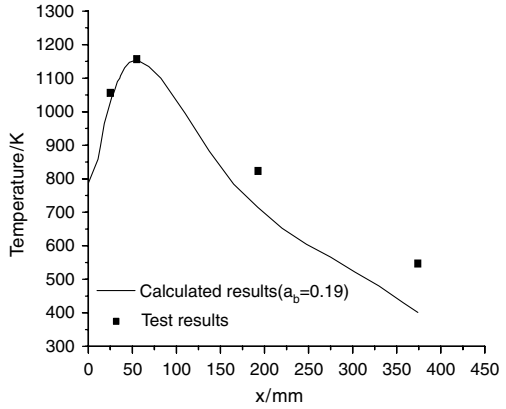

Fig. 5 Comparison between the temperatures of the test and the numerical simulation.

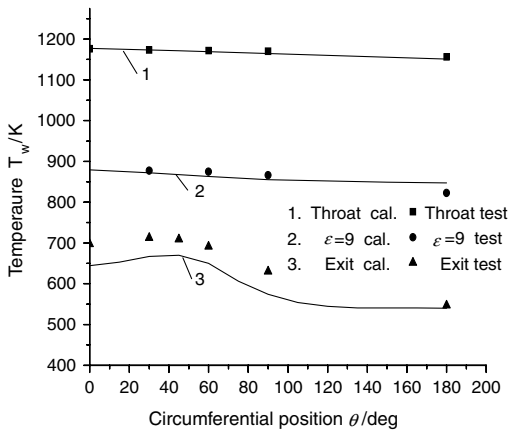

Fig. 6 Circumferential temperature distribution of the test data and numerical simulation at three axial positions.

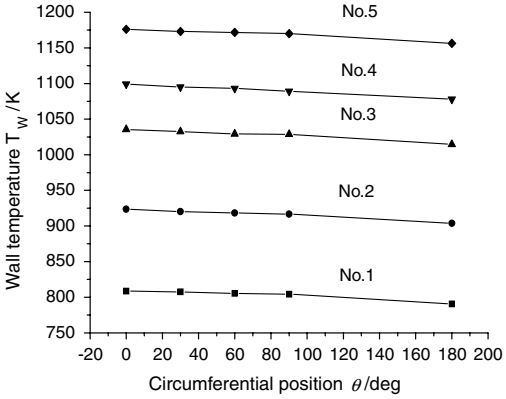

a) Circumferential temperature distribution

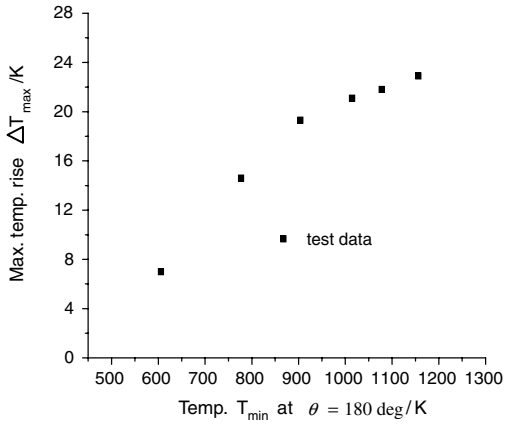

b) Variation of max. circumferential temperature rise with temperature T_{min} at θ = 180 deg (The first result from the left is acquired in the preheating process)

Fig. 7 Characteristics of temperature distribution at the throat with four electrically heated nozzles.

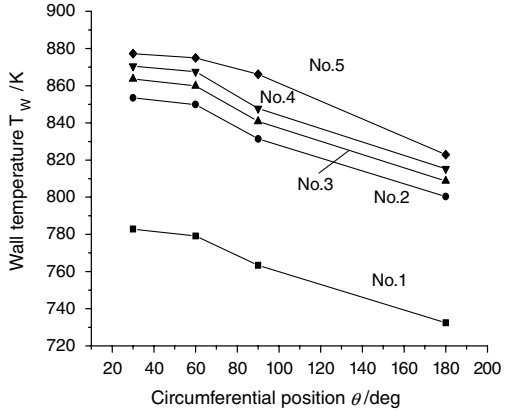

a) Circumferential temperature distribution

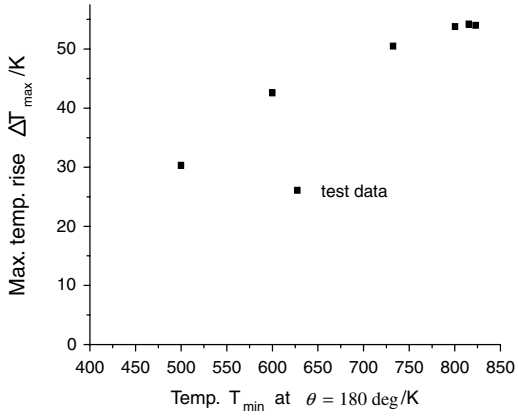

b) Variation of max. circumferential temperature rise with temperature T_{min} at θ = 180 deg (The first result from the left is acquired in the preheating process)

Fig. 8 Characteristics of temperature distribution at the beginning of the extension section ε = 9 with four electrically heated nozzles.

A. Comparison with Numerical Simulation Results

A numerical simulation of the temperature distribution of the four parallel engines with all-radiation cooling has been made in [3]. The liquid propellant used in the engine was unsymmetrical dimethylhydrazine/N_2O_4. First, the physical model was established and the node distribution was made according to some assumptions. Second, energy balance equations of the thrust chamber wall were developed by omitting radial heat conduction through the wall and considering the radiative heat transfer among the four nozzles, the radiation leakage through the nozzle exit, and the axial and circumferential heat conduction. The concepts of effective radiation and incident radiation were introduced to calculate radiative heat transfer among the four nozzles. The view factors among the whole system were obtained using the Monte Carlo method. Last, the wall temperature field of the four parallel high-altitude engines was acquired by solving two coupled nonlinear equations for temperature and effective radiation, respectively, using an iterative method with linearization.

Table 2 The power of the three heaters and heating time

	Heating power P/W with four/two working nozzles			Heating
No.	P_1	P_2	P_3	Time/min
1	300/800	800/1200	1200/1200	30/20
2	500/1000	1200/1200	1200/1200	15/20
3	800/1200	1200/1200	1200/1200	15/12
4	1000/1440	1200/1520	1200/1520	15/15
5	1200/1680	1200/1520	1200/1520	15/30

Figure 5 presents a comparison between the calculated results with a mixture ratio of $\alpha_b = 0.19$ and the axial wall temperature test data at $\theta = 180$ deg. It is indicated that the design of the electric heating in this paper is conservative. The test data curve is above that of the calculated results. Figure 6 presents a comparison of the circumferential temperature distribution between the numerical simulations and the test data at three axial positions on the nozzle: at the throat, at $\varepsilon = 9$, and at the exit of the nozzle. All four nozzles were heated simultaneously. The comparison indicates that the numerically simulated results coincide well with the test data on the whole. The maximum circumferential temperatures of the throat and the section $\varepsilon = 9$ are at the circle angle $\theta = 0$ deg and those of the exit section are at about the circle angle $\theta \approx 40$ deg. The temperature level of the extension section in the test is higher than that of the numerical simulation.

B. Test Results

1. Results with Four Parallel Nozzles Heated Simultaneously

Figure 7 presents the distribution of the circumferential wall temperature $T = f(\theta)$ at the throat with the five different electric heating powers shown in Table 2 and the variation of the maximum circumferential temperature rise $\Delta T_{max} = T_{max} - T_{min}$ at the throat with the temperature $T_{min} = T_{\theta=180\ deg}$. The figure shows that there are maximum and minimum circumferential temperatures at $\theta = 0$ and 180 deg, respectively, at all conditions. The maximum circumferential temperature rise ΔT_{max} increases with the increase of T_{min} at the throat, and the increasing trend gradually becomes weak. $\Delta T_{max} \approx 24$ K when $T_{min} = 1156$ K at the throat, which indicates that there is a finite temperature rise resulting from the radiative heat

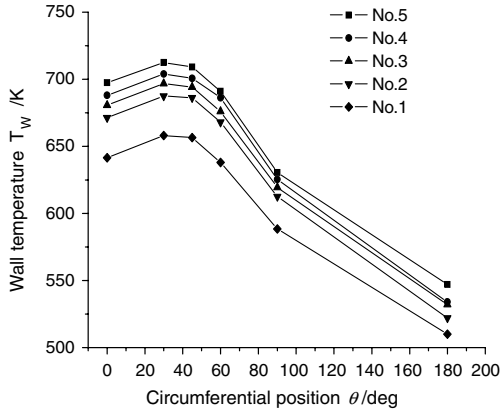

a) Circumferential temperature distribution

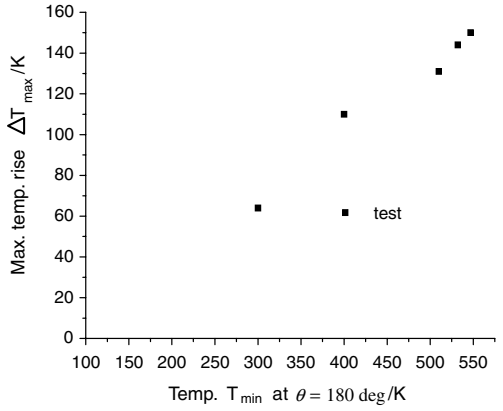

b) Variation of max. circumferential temperature rise with temperature T_{min} at θ = 180 deg

Fig. 9 Characteristics of temperature distribution at the exit with four electrically heated nozzles.

transfer among the four nozzles with high temperature at the throat. Figure 8 presents the distribution of circumferential wall temperature at the beginning of the extension section with $\varepsilon = 9$ and the variation of ΔT_{max} with T_{min}. There are the same variational characteristics as those at the throat, and the temperature rise is higher than that at the throat. ΔT_{max} is 53K as the corresponding T_{min} is 850K. Figure 9 presents the temperature results measured at the exit. Its variational characteristics are different from those at the throat. There are the maximum circumferential wall temperatures at approximately $\theta = 40$ deg, not $\theta = 0$ deg. ΔT_{max} is 155K as the corresponding T_{min} is 547K with the maximum heating power, which is far larger than that at the throat. According to the aforementioned analyses, we can conclude the following:

1) The circular angle θ, corresponding with the maximum circumferential wall temperature T_{max}, is dependent on the axial position, whereas the position of minimum circumferential wall temperature T_{min} is always at $\theta = 180$ deg.

2) The maximum circumferential temperature rise ΔT_{max} varies axially, and ΔT_{max} is smaller at the throat with high temperature, whereas ΔT_{max} is larger at the exit with low temperature.

Figure 10 is a photo of the test nozzles with $T_{min} = 1156$ K at the throat, taken by digital camera through the glass window on the vacuum cabin. It is obvious that the color of the test nozzles changes from yellow to red to dazzling white light during the test.

Calculation shows that the wall temperature of the throat and the exit at $\theta = 180$ deg is 1618 and 723K, respectively, for a mixture ratio in the region near the wall of 0.29 [3]. Extrapolation of the test data shows that the corresponding ΔT_{max} at the throat and the exit is about 30 and 250K, respectively.

Fig. 10 Four electric heating nozzles with $T_{min} = 1156$K taken outside cabin's window.

2. *Results with Two Diagonal Nozzles Heated Simultaneously*

Simultaneous firing of two engines arranged diagonally in this type of system is one of the propulsive modes for spacecraft to change orbit. Figures 11–13 present the results of circumferential wall temperature and maximum circumferential temperature rise measured at different axial positions. A comparison of these results to the results of four parallel nozzles heated simultaneously indicates that 1) the maximum and minimum circumferential temperatures are $\theta = 0$ and 180 deg, respectively, at different axial positions; and 2) ΔT_{max} increases as T_{min} increases. However, ΔT_{max} is less than that of the four parallel nozzles heated simultaneously.

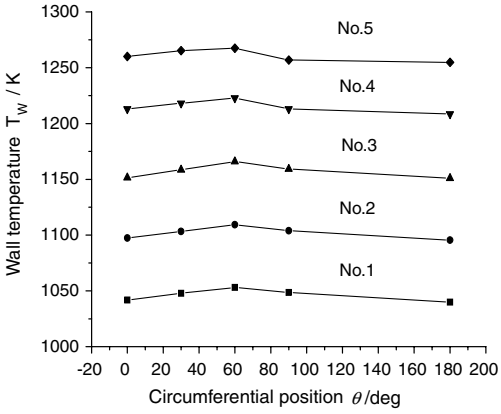

a) Circumferential temperature distribution

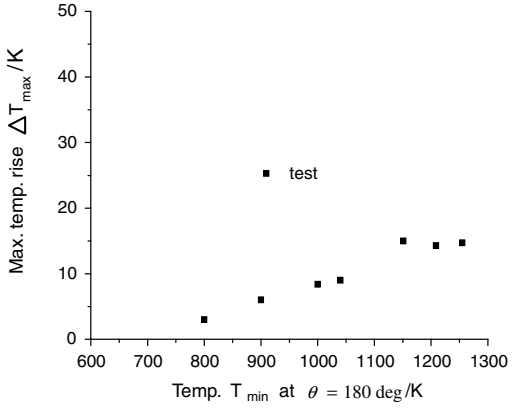

b) Variation of max. circumferential temperature rise with temperature T_{min} at θ = 180 deg (the first two results located at the left are acquired in the preheating process)

Fig. 11 Characteristics of temperature distribution at the throat with two electrically heated nozzles.

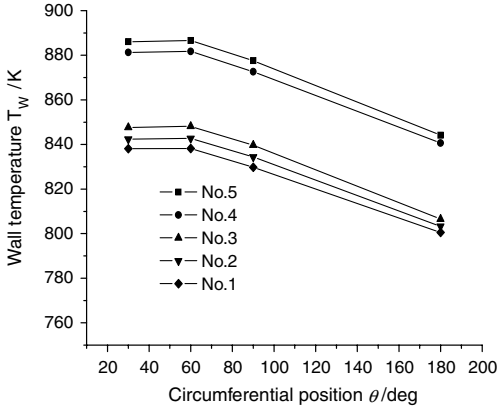

a) Circumferential temperature distribution

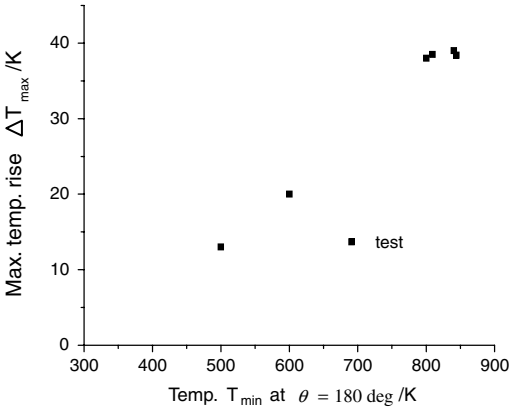

b) Variation of max. circumferential temperature rise with temperature T_{min} at θ = 180 deg (the first result located at the left is acquired in the preheating process)

Fig. 12 Characteristics of temperature distribution at the beginning of the expansion section $\varepsilon = 9$ with two electrically heated nozzles.

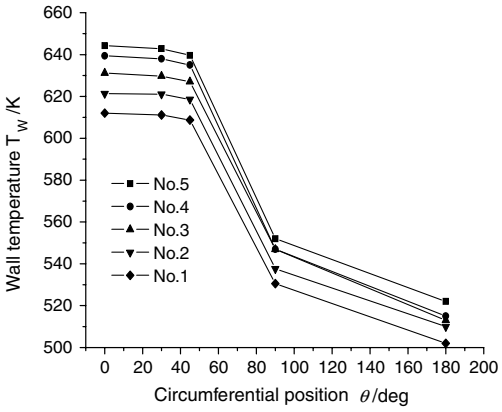

a) Circumferential temperature distribution

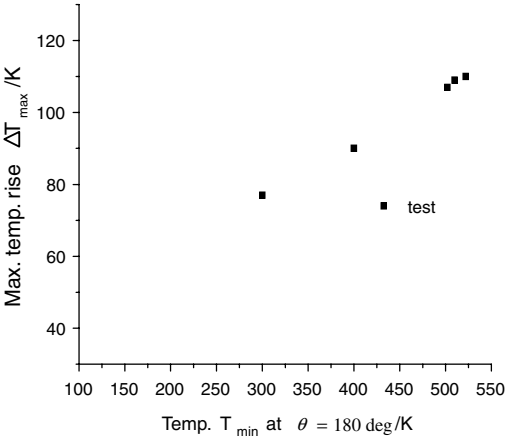

b) Variation of max. circumferential temperature rise with temperature T_{min} at θ = 180 deg

Fig. 13 Characteristics of temperature distribution at the exit with two electrically heated nozzles.

V. Error Analysis

The errors in this simulation test include temperature measurement error and circumferential wall temperature difference.

A. Error Analysis for Temperature Measurement

The measurement error is made up of acceptable errors of the thermocouples and errors caused by material asymmetry of the thermocouple and secondary instruments (data collection system).

According to the national criterion, the accepted error of the platinum–PRA thermocouple is $\pm 0.25\%\, t$ with a temperature range from 600 to 1600°C, whereas that of the NCA–NSA thermocouple is $\pm 0.75\%\, t$ with a temperature range from −40 to 1600°C [12], where t is the measured temperature (unit is degrees Celsius). Errors caused by material asymmetry of the platinum–PRA thermocouple and the NCA–NSA thermocouple are all less than 0.2°C, which is negligible. The data collection system is an HP3054. The secondary instrument error for the platinum–PRA thermocouple with a temperature range from 600 to 1200°C is ±1.5–1.8 °C [12], and the relative error is $0.18\%\, t$. The secondary instrument error for the NCA–NSA thermocouple with a temperature range from 300 to 900°C is ±0.7–0.9 °C [12], and the relative error is $0.2\%\, t$. Consequently, the maximum measurement error is $0.43\%\, t$ for the platinum–PRA thermocouple and $0.95\%\, t$ for the NCA–NSA thermocouple.

B. Error Analysis of Circumferential Wall Temperature Difference

The circumferential wall temperature difference ΔT is defined as the temperature value at a certain circumferential position at a certain axial section of the test nozzle minus the minimum temperature value of the section. According to the error algorithm [13], the error for circumferential temperature difference should be twice as large as the measurement of the temperature wall; therefore, the maximum error for ΔT is $\pm 0.43\%\, t \times 2 = \pm 0.86\%\, t$ for the platinum–PRA thermocouple and $0 \pm .95\%\, t \times 2 = \pm 1.9\%\, t$ for the NCA–NSA thermocouple. The error for ΔT also results from an eccentric installation of heaters against the nozzle, which is about $0.88\%\, t$. Thus, the maximum error is $(0.86\% + 0.88\%)t = 1.74\%\, t$ (root mean square error is $1.04\%\, t$) for the platinum–PRA thermocouple and $(1.9\% + 0.88\%)\, t = 2.78\%\, t$ (root mean square error is $2.15\%\, t$) for the NCA–NSA thermocouple.

VI. Conclusions

1) A new scheme exists for ground simulation testing in a vacuum cabin with normal temperature, which can be used to evaluate the influence of radiative heat transfer among high-temperature nozzles in space. Enhancing the vacuum degree of the cabin is a key means to the test's success.

2) Testing data have proven that a circular angle with a maximum circumferential wall temperature T_{max} is dependent on the axial position, whereas the minimum circumferential wall temperature T_{min} is consistently at $\theta = 180$ deg when four parallel nozzles work simultaneously. Maximum and minimum circumferential temperatures are $\theta = 0$ and 180 deg, respectively, at different axial positions when two diagonal nozzles work simultaneously. The maximum circumferential temperature rise ΔT_{max} increases with the increase of T_{min} in these two conditions. The temperature difference ΔT_{max} as four parallel nozzles work simultaneously is larger than ΔT_{max} as two diagonal nozzles work simultaneously.

3) It is shown from extrapolation of the testing data that the wall temperature T_{min} of the throat is 1618K, while ΔT_{max} is only about 30K. There is a small circumferential temperature rise in the high-

temperature throat. The temperature difference $\Delta T_{\max}$ of the exit is larger (about 250K), whereas the wall temperature is smaller (about 723K). So the wall temperature rise in the nozzles of four parallel engines in space does not affect the normal working of engines.

4) On the whole, the test data coincide well with the numerically simulated results. The design of the electric heating in this paper is conservative relative to the actual engines.

Acknowledgment

The authors are grateful for the support of the Science and Technology Commission of Shanghai Municipality (award no. 08R21420300).

References

[1] Lu, W. C., Cheng, H. E., and Li, B. C., "Effect of Integration on Temperature Distribution of Radiation Surfaces," *Journal of Engineering Thermophysics*, Vol. 19, No. 6, 1998, pp. 732–735 (in Chinese).

[2] Schoenman, L., Rosenberg, S. D., and Jassowski, D. W., "Test Experience, 490-N High-Performance [321-s Specific Impulse] Engine," *Journal of Propulsion and Power*, Vol. 11, No. 5, 1995, pp. 992–997.

[3] Niu, L., Cheng, H. E., Zang, J. L., and Huang, R. S., "Influence of Outward Radiation of Four Parallel Thrust Chambers on Wall Temperature," *Journal of Propulsion Technology*, Vol. 21, No. 6, 1999, pp. 14–17 (in Chinese).

[4] Cheng, H. E., and Niu, L., "Analysis of Heat Transfer for Thrust Chambers of Four Parallel Engines by All Radiation Cooling," *Journal of Shanghai Jiaotong University*, Vol. 33, No. 8, 1999, pp. 974–978 (in Chinese).

[5] Baehr, H., and Stephan, D. K., *Heat and Mass-Transfer*, Springer, New York, 2006.

[6] Robert, S., and John, R. H., *Thermal Radiation Heat Transfer*, Taylor and Francis, New York, 2002.

[7] Gilmore, D. G., *Spacecraft Thermal Control Handbook*, Aerospace Press, El Segundo, CA,2002.

[8] Cheng, B. J., Guo, X. Z., and Yang, H., etc, "Effects of Zircon Additive on the Properties of 95-Alumina Ceramic," *Key Engineering Materials*, Vols. 280–283, No. II, 2005, pp. 1013–1016.

[9] Kou, S., *Welding Metallurgy*, Wiley, Hoboken, NJ, 2003.

[10] Huang, B. C., and Ma, Y. L., *Space Environment Test Technology of Spacecraft*, National Defence Industry Press, Beijing, 2002 (in Chinese).

[11] Tremante, A., and Malpica, F., "Analysis of the Temperature Profile of Ceramic Composite Materials Exposed to Combined Conduction-Radiation Between Concentric Cylinders," *Journal of Engineering for Gas Turbines and Power*, Vol. 120, No. 2, 1998, pp. 271–275. doi:10.1115/1.2818115

[12] Li, S. R., and Ling, S. K., *Foundation of the Temperature Measure*, Chinese National Criterion Press, Beijing, 1998 (in Chinese).

[13] Sha, D. G., *Error Analysis and Evaluation of Uncertainty Degree for The Measurement*, Chinese Measurement Publishing House, Beijing, 2003 (in Chinese).

D. Talley
Associate Editor